Toward a Stretchable, Elastic, and Electrically Conductive Nanocomposite: Morphology and Properties of Poly[styrene-*b*-(ethylene-*co*-butylene)-*b*-styrene]/Multiwalled Carbon Nanotube Composites Fabricated by High-Shear Processing

Yongjin Li* and Hiroshi Shimizu

Nanotechnology Research Institute, National Institute of Advanced Industrial Science and Technology (AIST), Tsukuba Central 5, 1-1-1 Higashi, Tsukuba, Ibaraki 305-8565, Japan

Received December 1, 2008; Revised Manuscript Received February 9, 2009

ABSTRACT: Nanocomposites based on a thermoplastic elastomer, poly[styrene-*b*-(ethylene-*co*-butylene)-*b*-styrene] triblock copolymer (SEBS), and multiwalled carbon nanotubes (MWCNTs) were fabricated using a high-shear processing technique. The MWCNTs were homogeneously dispersed in the SEBS matrix, even at an MWCNT concentration of 15 wt %. The addition of MWCNTs to the elastomer significantly enhanced its electrical conductivity and mechanical properties, including increased modulus and tensile strength, with only a slight loss of stretchability. The fabricated nanocomposites loaded with 15 wt % MWCNT showed an excellent stretchability of more than 600% and a high strain recovery under mechanical deformation. Moreover, the conductivity of fabricated conductive nanocomposites only slowly decreases with uniaxial stretching. Therefore, a stretchable and elastic conductive polymer nanocomposite was successfully fabricated. In addition, the effect of the uniformly dispersed MWCNTs on the SEBS microphase separation behaviors was also investigated by small-angle X-ray scattering (SAXS), synchrotron SAXS, and transmission electron microscopy (TEM). The results indicate that the homogeneously dispersed MWCNTs not only disturb the microphase-separated structure of SEBS but also decrease its order−disorder transition temperature.

1. Introduction

Electrically conductive elastomers have been widely used in various fields including electromagnetic shielding, seals, and electrostatic paintings. The addition of conductive fillers, such as carbon black, carbon fiber, or metallic particles, into an elastomer (or rubber) matrix is the easiest method of fabricating conductive elastomers. An electrical pathway is established by the formation of a conductive filler network. Therefore, the electrical conductivity of the produced composites is mainly determined by the filler loading content, dispersion, aspect ratio, and the interaction between the filler and the matrix. Relatively large volume fractions (>30 wt %) of fillers are necessary to obtain the desired conductivity for conventional conductive fillers, but this inevitably has a negative impact on other properties of the composites, such as the elasticity, deformability, surface finish, and processability.[1,2] Recently, soft and stretchable materials with high electrical conductivity have attracted significant attention because they may be used to create stretchable electronic circuits.[3,4] Clearly, traditional conductive fillers cannot be adapted to satisfy the requirements of such applications.

Carbon nanotubes (CNTs) are considered to be ideal conductive filler owing to their large aspect ratios, nanoscale diameter, and very high electrical conductivity along the tube axis. The significantly enhanced electrical conductivity in polymer (mainly in the glassy state)/CNT composites upon the small loading of nanotubes in the polymer matrix has been reported in many studies.[5−11] The extremely low percolation threshold of polymer/CNT nanocomposites not only provides materials with electrical conductivity similar to conventional filled systems but also maintains the performance of the matrix polymer, such as its mechanical properties, optical clarity, and processability. Therefore, CNTs are expected to be the best conductive fillers for an elastomer matrix to fabricate stretchable conductive nanocomposites because the stretchability of the matrix elastomer should be maintained upon small CNT loading. Vaia et al.[12,13] fabricated thermoplastic polyurethane (PU) elastomer/multiwalled carbon nanotube (MWCNT) composites and found that addition of less than 10 vol % MWCNTs to PU resulted in an elastomer nanocomposite with an electrical conductivity of about 1−10 S/cm without loss of the elongation at break of the matrix. Very recently, Sekitani et al.[14] reported the fabrication of uniformly dispersed single-walled carbon nanotube (SWCNT) nanocomposites in a fluorine rubber by solution blending with the aiding of an ionic liquid. The prepared nanocomposites exhibited extremely high conductivity and a stretchability of more than 100%. On the other hand, Huang et al.[15,16] produced stretchable films where wavy SWCNTs are embedded in a poly(dimethylsiloxane) (PDMS) matrix. However, almost all of these nanocomposites were prepared by solution blending or even more complicate methods which have obvious limitations for industrial applications in terms of both cost and environmental impact. We have successfully dispersed pristine MWCNTs in poly(vinyldiene fluoride)[17] and poly(styrene-*b*-butylene-*co*-butadiene-*b*-styrene)[18] matrixes by melt blending using a high-shear extruder. Our investigation showed that the dispersion of MWCNTs in the polymers was greatly dependent on the shear stress exerted during the melt blending, and very strong correlations between the processing conditions, morphologies, and properties were obtained for the processed nanocomposites.

In this work, a thermoplastic elastomer, poly[styrene-*b*-(ethylene-*co*-butylene)-*b*-styrene] triblock copolymer (SEBS), was compounded with MWCNTs by melt blending using a high-shear extruder with the aim of fabricating highly conductive nanocomposites with excellent stretchability and elasticity. The morphological analysis and the evaluation of the physical properties were carried out on the fabricated nanocomposites with various amounts of MWCNT loading. We also focused on the effects of dispersed MWCNTs on the microphase

* To whom correspondence should be addressed. E-mail yongjin-li@aist.go.jp.

10.1021/ma802662c CCC: $40.75
Published on Web 03/04/2009

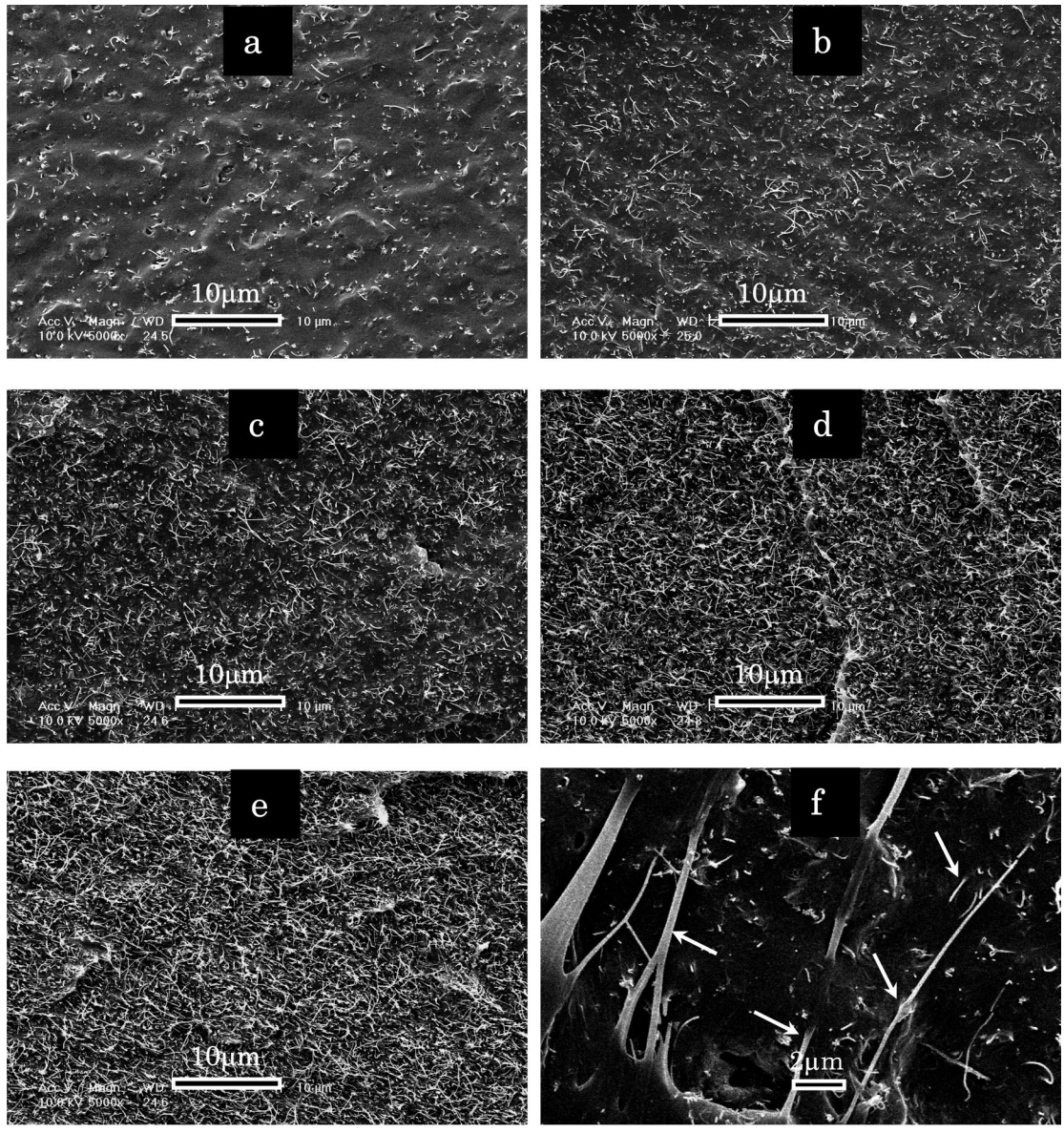

Figure 1. SEM images of SEBS/MWCNT nanocomposites with different nanotube loadings: (a) 1.25, (b) 2.5, (c) 5.0, (d) 10, (e) 15, and (f) 1.25 wt % at higher magnification.

separation of the matrix as well as the correlation between the morphology and the properties upon uniaxial deformation.

2. Experimental Section

2.1. Materials and Sample Preparation. The SEBS block copolymer was bought from Asahi Kasei Corp. (Japan), and the weight ratio of styrene:ethylene−butylene was 30:70. The high-purity MWCNTs (about 95%) were kindly provided by Nikkiso Co., Ltd. (Japan). The tube diameters were in the range of 10−30 nm with lengths of 10−20 μm. The MWCNTs were used as received without further treatment. SEBS composites containing various amounts of MWCNTs were prepared via a melt-compounding method using an HSE3000 mini high-shear extruder (Imoto, Japan).[19] The rotation speed of the screw used in this study was set to 1000 rpm, which corresponds to the average shear rate of around 1500 s^{-1} at the region of top part of the screw. The melt compounding was carried out at 200 °C for 2 min using the extruder. The compounded samples were then extruded from a T-die. For the measurements of mechanical properties, all the extruded samples were hot-pressed at 200 °C to a sheet with a thickness of 500 μm, followed by cooling to room temperature.

2.2. Morphological Characterization. The dispersion of MWCNTs in the SEBS matrix was observed using a field emission scanning electron microscope (FE-SEM). A Philips XL-20 SEM was used for the measurements at an accelerating voltage of 10 kV. All the samples were fractured by immersion in liquid nitrogen for about 10 min. The fracture surface was then coated with a thin layer of gold before the observation. To investigate the effects of MWCNTs on the microphase separation of the matrix SEBS, transmission electron microscopy (TEM) was performed using a Hitachi H7000 instrument operating at an acceleration voltage of 75 kV. The composite sample was ultramicrotomed at −120 °C to a section with a thickness of about 70 nm. The sections were then stained using osmium tetroxide (OsO_4) for 12 h.

Small-angle X-ray scattering (SAXS) patterns were obtained using microfocused Cu Kα radiation (45 kV, 60 mA) generated by an X-ray diffractometer (Rigaku Ultrax 4153A 172B) and an imaging plate detector. The exposure time was 3 h for each measurement. The Lorentz corrections were performed after subtraction of the air scattering. Changes in the scattering intensities of neat SEBS and its nanocomposites during heating (2 °C/min) were studied by real-time SAXS measurements, which were conducted at the BL-10C beamline in the Photon Factory of the High-Energy Accelerator Research Organization (Tsukuba, Japan).

2.3. Properties Measurements. Dynamic mechanical analysis (DMA) was carried out using a Rheovibron DDV-25FP (Orientec

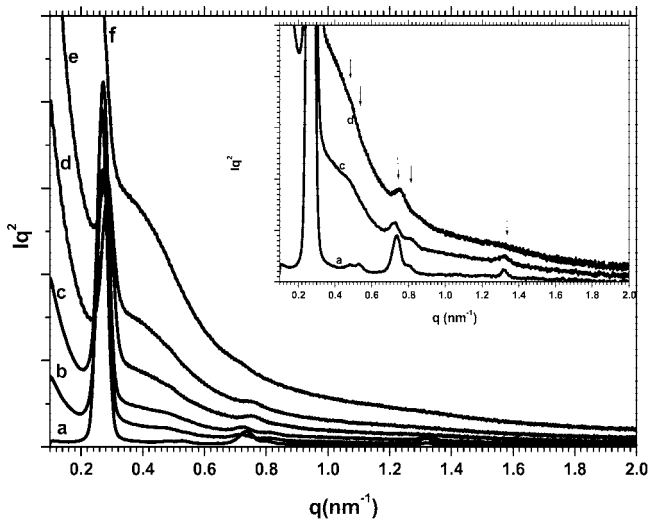

Figure 2. Lorentz-corrected SAXS profiles for neat SEBS and its nanocomposites: (a) neat SEBS, (b) with 1.25 wt % MWCNTs, (c) with 2.5 wt % MWCNTs, (d) with 5 wt % MWCNTs, (e) with 10 wt % MWCNTs, and (f) with 15 wt % MWCNTs. (The inset is an enlarged profile to show the multiple scattering peaks.)

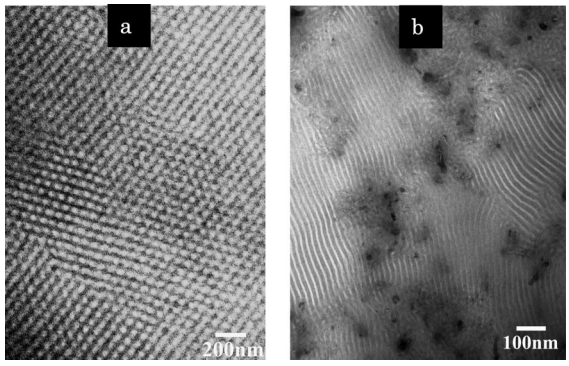

Figure 3. TEM images for (a) neat SEBS and (b) SEBS with 1.25 wt % MWCNTs.

Corp., Japan) in the tensile mode. Dynamic loss (tan δ) was determined at a frequency of 1 Hz and a heating rate of 3 °C/min as a function of temperature from −150 to 175 °C.

Tensile tests were carried out in accordance with the ASTM D 412-80 test method using dumbbell-shaped samples punched out from the molded sheets. The tests were performed using a tensile testing machine, Tensilon UMT-300 (Orientec Co., Ltd., Japan), at a crosshead speed of 50 mm/min at 20 °C and 50% relative humidity. Strain-recovery tests were performed using the same machine as follows. After the preset strain (200% elongation) was attained, the crosshead was returned at the same speed as that when stretching until zero stress was reached. Successive tensile tests were also carried out using the same equipment and measuring conditions as those of the strain recovery test, but gradually increasing the preset strain from 25% to 125% with the internal of 25%. The measured sample was relaxed at room temperature for 60 min, and then the next strain recovery test was started.

Two types of characterization apparatus were used in evaluating the electrical conductivity of the prepared composites depending on the conductivity of the samples. For samples with high resistivity, an Advantest R8340A ultrahigh-resistance meter was used. Different voltages were applied to different samples depending on the level of resistivity of the specimens. For samples with high conductivity, the resistivity of the samples was measured in accordance with the JIS K7194 method (a method for testing the resistivity of conductive plastics using a four-point probe array). The conductivity of the nanocomposites under stretching was measured as follows. After the samples were stretched to the preset strain and kept under the strain for about 10 s, the measurements were conducted using a four-point probe parallel to the stretching direction.

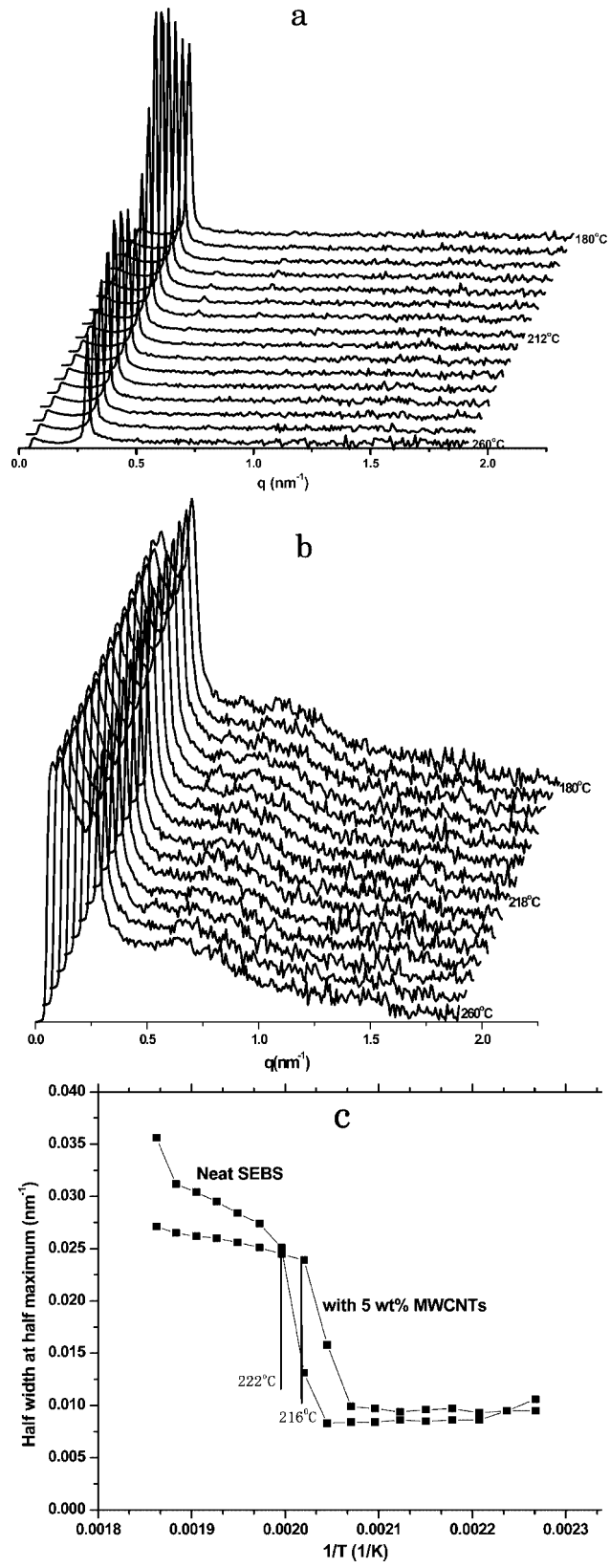

Figure 4. (a) SAXS profiles as a function of temperature for neat SEBS (heat rate 2 °C/min), (b) SAXS profiles as a function of temperature for SEBS nanocomposite with 5 wt % MWCNTs (heat rate 2 °C/min), and (c) relationships between the half-width at half-maximum and the reciprocal temperature for the indicated samples.

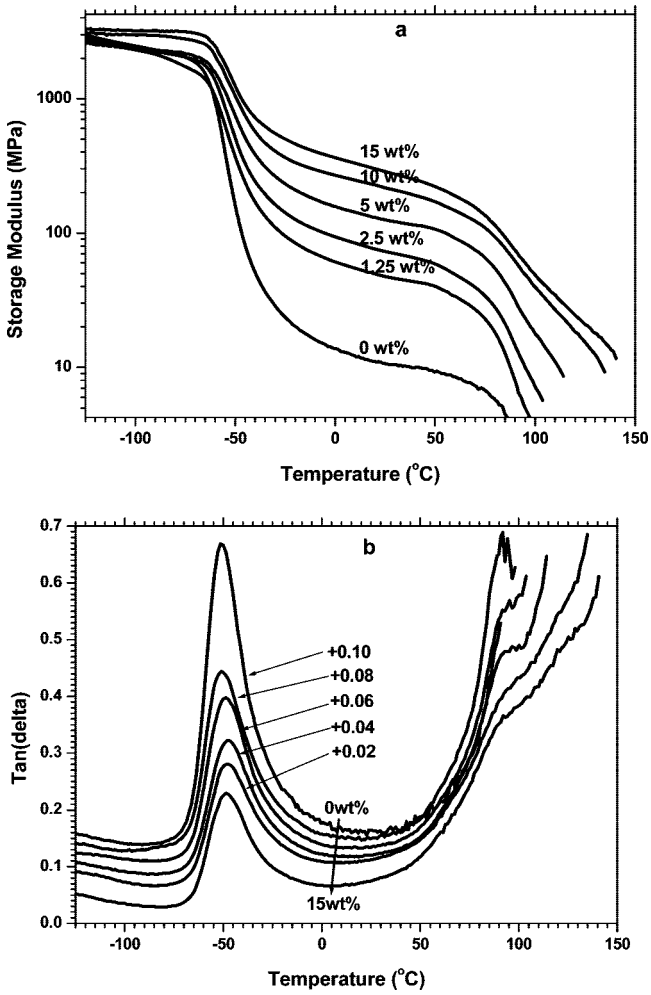

Figure 5. Temperature dependence of (a) storage modulus and (b) tan δ for the SEBS/MWCNT nanocomposites with indicated MWCNT loadings.

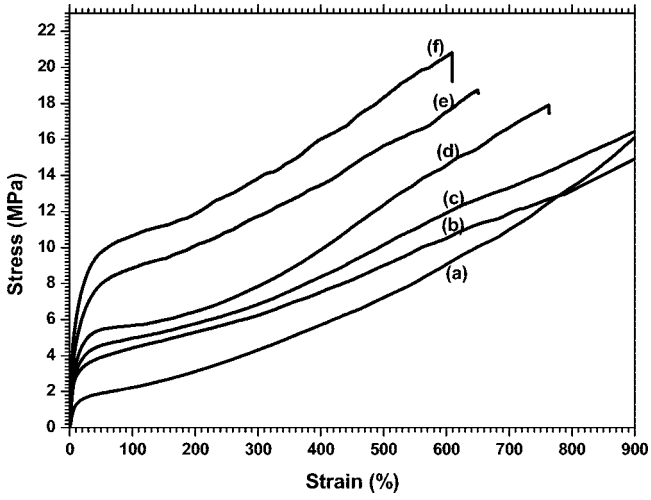

Figure 6. Strain−stress curves for (a) neat SEBS, (b) with 1.25 wt % MWCNTs, (c) with 2.5 wt % MWCNTs, (d) with 5 wt % MWCNTs, (e) with 10 wt % MWCNTs, and (f) with 15 wt % MWCNTs.

3. Results and Discussion

3.1. Dispersion of MWCNTs in the SEBS Matrix. It is well-known that the homogeneous dispersion of the filler and the strong interfacial interaction between the filler and the polymer matrix can effectively improve the mechanical, electrical, and thermal performances of the prepared composites. Our previous investigations have shown that the shear stress exerted on the CNTs has a critical role in improving their dispersion and that homogeneously dispersed CNTs can be obtained upon increasing the screw rotation speed during melt compounding.[17,18] Figure 1 shows SEM images of the SEBS/MWCNT nanocomposites

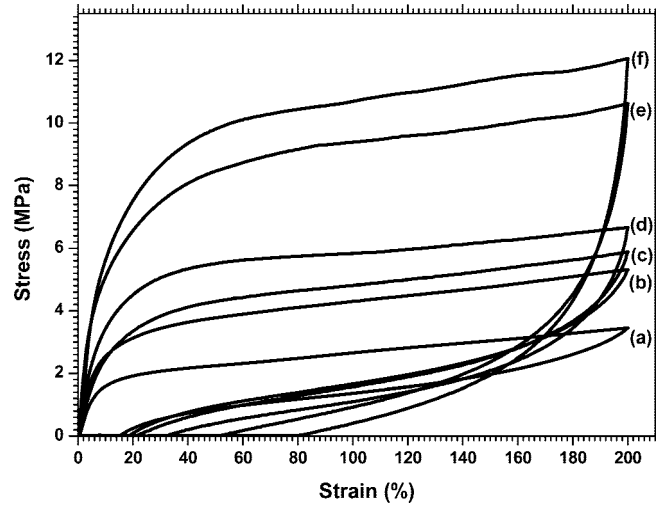

Figure 7. Strain-recovery curves for (a) neat SEBS, (b) with 1.25 wt % MWCNTs, (c) with 2.5 wt % MWCNTs, (d) with 5 wt % MWCNTs, (e) with 10 wt % MWCNTs, and (f) with 15 wt % MWCNTs.

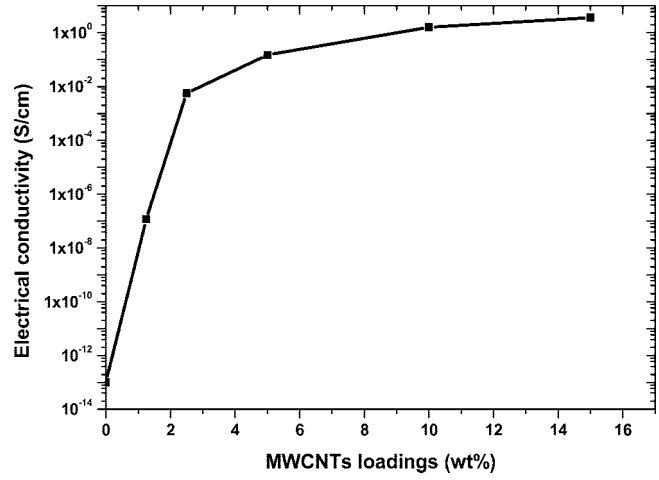

Figure 8. Electrical conductivity of SEBS/MWCNT nanocomposites as a function of CNT loading.

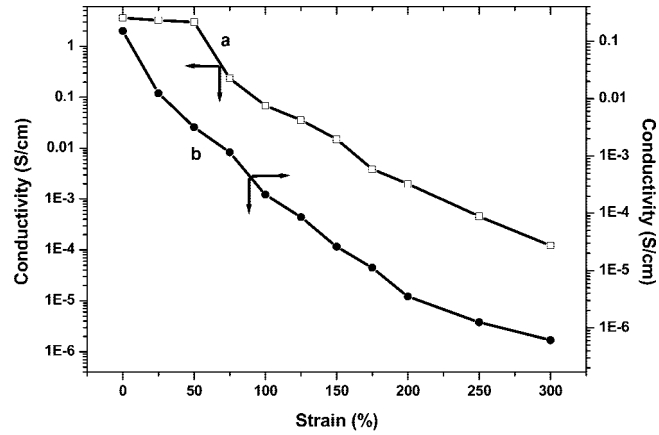

Figure 9. Electrical conductivity of SEBS/MWCNT nanocomposites as a function of uniaxial tensile strain: (a) with 15 wt % MWCNTs and (b) with 5 wt % MWCNTs.

prepared using the high-shear extruder at a screw rotation speed of 1000 rpm. It can be seen that the MWCNTs are uniformly dispersed in the SEBS matrix at the MWCNT loadings investigated here. No MWCNT agglomerates are apparent even at the very high MWCNT content of 15 wt %. The uniform dispersion of the pristine MWCNTs can be attributed to the high shear stress exerted by the high-shear extruder during mixing. The shear stress may overwhelm the electrostatic and van der Waals interactions between the nanotubes and peel each nanotube apart. Torkelson et al. found that an external mechanical force can also induce the regular dispersion of CNTs in a polypropylene matrix.[20] On the other hand, it can be seen from Figure 1a that the MWCNTs are separated from each other and the MWCNT network is still incomplete in the sample with 1.25 wt % MWCNTs. However, the entanglement of MWCNTs can be observed, and a satisfactory nanotube network is formed upon adding 2.5 wt % MWCNTs (Figure 1b). Further increasing the loading content leads to the greater entanglements of CNTs in the SEBS matrix and higher CNT network density.

The fracture surface of the nanocomposite with 1.25 wt % CNTs was examined at higher magnification to evaluate the adhesion between the MWCNTs and the matrix. Some discrete nanotubes, apparently pulled out together with the matrix polymer during fracturing, can be distinguished (see the arrows in Figure 1f). This indicates the strong interfacial adhesion between the MWCNTs and the SEBS matrix.

3.2. Effects of Dispersed MWCNTs on the Phase Structure of SEBS. As a block copolymer, SEBS undergoes microphase separation into self-assembled ordered morphologies with a size of less than 100 nm.[21,22] The diameter of CNTs used is ~20 nm, which is comparable to the size of the microphase-separated domains of the SEBS matrix. Therefore, it is very interesting to investigate the effects of the well-dispersed MWCNTs on the SEBS phase structure. Figure 2 shows Lorentz-corrected SAXS profiles for neat SEBS and its nanocomposites. Neat SEBS produces strong multiple scattering peaks with q ratios of $1:\sqrt{3}:\sqrt{4}:\sqrt{7}:\sqrt{9}$..., indicating a typical hexagonal-packed cylindrical microstructure. For the nanocomposites with less than 5 wt % MWCNTs, multiple scattering peaks with almost the same peak positions as neat SEBS were observed, which suggests that the well-dispersed MWCNTs do not change the morphology of microphase-separated SEBS and that the SEBS matrix maintains the cylindrical structure in the nanocomposites. However, the fact that fewer scattering peaks with greater width were observed with increasing MWCNT loading means that the size of the phase-separated grains decreases[23] when well-dispersed MWCNTs exist inside. It is considered that MWCNTs impede the formation of large phase-separated grains of SEBS, and only small grains are located in the spaces between the neighboring MWCNTs in the nanocomposites. For the nanocomposites with 10 and 15 wt % MWCNTs, very limited space was available for the growth of phase-separated grains due to the extremely high MWCNT concentration. No well-developed grains with regular structures formed. Therefore, only the first-order scattering peak was observed at these concentrations, as shown in Figure 2. Note that all the nanocomposites exhibit a very strong diffused scattering at a low angle ($q < 0.2$ nm^{-1}) and that the intensity of the scattering increases gradually with increasing MWCNT content. The scattering originates from the randomly dispersed MWCNTs. The same phenomenon has also been observed for some other nanoparticle-filled polymer systems.[24−26]

The spatial confinement for the growth of phase-separated grains due to the exfoliated MWCNTs was confirmed by TEM. Figure 3 shows TEM images for neat SEBS and its nanocomposite with 1.25 wt % MWCNTs. The neat SEBS has the perfect hexagonal-packed cylinders vertical to the paper plane. In contrast, a disordered structure was observed in the region near the MWCNTs in the nanocomposite, but a highly ordered phase structure is still formed far from the MWCNTs. It is thus concluded that the dispersed MWCNTs (black dots in the TEM image) suppress the formation of the phase-separated structure of SEBS. The TEM results are consistent with those observed from SAXS.

All the block copolymers undergo order−disorder transitions, in which a heterogeneous miscrophase-separated melt is transformed into a homogeneous melt with increasing temperature.[23] The transition temperature, T_{ODT}, is an important physical parameter for block copolymers. Both the static SAXS and TEM results indicate that the long-range order of SEBS is suppressed by the highly dispersed MWCNTs. It is therefore important to determine the effects of MWCNTs on the order−disorder transitions of the SEBS matrix. Parts a and b of Figure 4 show the temperature-dependent SAXS profiles for neat SEBS and the nanocomposite with 5 wt % MWCNTs, respectively. For both samples, abrupt changes in the scattering peak intensity and the half-width at half-maximum of the first scattering peak were observed, indicating the order−disorder transitions for SEBS upon increasing temperature. The temperature at which the half-width at half-maximum suddenly drops is defined as T_{ODT}, as shown in Figure 4c. It can be observed that the presence of MWCNTs depresses T_{ODT} from 222 to 216 °C. The depression of T_{ODT} has also been observed for polyhedral oligomeric silsesquioxane (POSS) grafted poly(styrene-*b*-butadiene-*b*-styrene) (SBS) systems.[27,28]

3.3. Dynamic Mechanical Analysis. Figure 5 shows the variation of storage modulus and the loss tangent as a function of temperature for neat SEBS and the nanocomposites with various nanotube loadings. It is clear from Figure 5a that the storage modulus values for nanocomposites are higher than that for neat SEBS over the whole temperature range. At low temperatures, SEBS is in the glassy state, and only a slight increase in the storage modulus was observed for the nanocomposites as compared with neat SEBS. With increasing temperature the modulus suddenly drops by several orders of magnitude corresponding to the glass transition of the EB block at about −50 °C. Above this temperature, all the nanocomposites exhibit a marked increase in the storage modulus with increasing MWCNT loading. The modulus at 25 °C for the nanocomposite with 15 wt % MWCNTs is 29 times higher than that of the pure SEBS. Note that the nanocomposites with high MWCNT content (>5 wt %) exhibit greatly improved thermal resistance. Neat SEBS starts to flow (modulus tends to 0) when the temperature is higher than 75 °C. However, a significant difference in the DMA curves was observed for the nanocomposites with more than 2.5 wt % MWCNTs. These samples are self-supporting at the high temperatures above that at which the SEBS matrix starts to flow due to the formed MWCNTs networks, which is consistent with the SEM results shown in Figure 1.

The variation of loss tangent (Figure 5b) for neat SEBS and the nanocomposites with temperature shows an EB glass transition at a temperature of about −50 °C. The transition temperature of the nanocomposites with more than 2.5 wt % CNTs is around −47 °C, which is higher than −50.7 °C for neat SEBS and the nanocomposite with 1.25 wt % nanotubes. The increased glass transition of EB block can be again attributed to the geometrically confined environments by the well-dispersed MWCNTs. Similar results have also been found for other nanocomposites using nanosilica[29,30] and nanoclay[31−33] as the fillers.

3.4. Mechanical Properties. The deformation behavior of carbon nanotubes has been investigated theoretically.[34] Figure 6 illustrates the strain−stress curves for neat SEBS and its

Table 1. Mechanical and Thermal Properties of SEBS and Its Nanocomposites with MWCNTs

MWCNT loading (wt %)	modulus (MPa)	300% tensile stress (MPa)	elongation at break (%)	strain residual (%)	T_g of EB phase (°C)
0	16.3	4.22	949	14.7	−50.7
1.25	35.6	6.27	927	18.2	−50.7
2.5	39.9	6.80	916	22.7	−48.2
5	75.8	7.79	765	30.7	−47.2
10	118.2	11.66	651	51.2	−47.6
15	185.8	13.83	611	76.2	−47.6

Table 2. Changes of the Tensile Modulus (in MPa) with the Previous Strain for the SEBS/MWCNT Nanocomposites Measured from Cyclic Tensile Tests

	previous strain (%)				
MWCNT loading (wt %)	0	25	50	75	100
5	75.8	46	34.2	30.1	25.6
15	185.8	173.1	160.4	81.4	48.8

nanocomposites. It is clear that the added MWCNTs show dramatic reinforcement effects for SEBS matrix because all the nanocomposites have a higher modulus and greater strength than neat SEBS. This strengthening effect increases with increasing MWCNT loading. Interestingly, all the nanocomposites show excellent stretchability as evidenced by the very high elongation at break. Moreover, the stretchability of the nanocomposites only slightly decreases upon increasing the MWCNT content, in contrast to most inorganic filler strengthened polymer systems.[35,36]

The elasticity is the main characteristic of elastomeric materials. The effects of MWCNTs on the elasticity of SEBS were investigated by strain-recovery measurements. The samples were first stretched at a crosshead speed of 50 mm/min and then unloaded at the same speed to a stress of 0. Figure 7 shows the strain-recovery curves for neat SEBS and the nanocomposites. Neat SEBS exhibits excellent elasticity with a residual strain of about 15%. With the addition of MWCNTs, the residual strain increases gradually, indicating the decreased elasticity of the nanocomposites. Two factors may account for the decreasing elasticity of the nanocomposites. On the one hand, the elasticity of the SEBS originates from the physical cross-linking network with the rigid PS nanodomains as the cross-link points. Both SAXS and TEM investigations show that the MWCNTs disturb the microphase separation behavior of SEBS. Therefore, the cross-link density may decrease gradually upon the incorporation of MWCNTs. On the other hand, there is no covalent bonding connection between the MWCNT surface and SEBS even though strong interfacial adhesion has been observed. An irreversible slip is highly likely to occur between the MWCNT surface and SEBS upon mechanical deformation. Although the MWCNTs deteriorate the elastic properties of SEBS, all the nanocomposites still show good strain-recovery properties. The residual strain of the nanocomposite with 15 wt % MWCNTs is 76% after 200% stretching, which means that about 62% of the deformation is recovered. The main mechanical properties and the glass transition temperature of the EB phase for neat SEBS and its nanocomposites are tabulated in Table 1.

3.5. Electrical Conductivity. Figure 8 shows the volume conductivities for SEBS/MWCNT nanocomposites as a function of the MWCNT loading content. As expected, the electrical conductivity of all the composites strongly depends on the nanotube loading content. A sudden increase in the conductivity was observed as the MWCNT loading content increased from 1.25 to 2.5 wt %, indicating the formation of a percolating network. The carbon nanotubes are entangled in the matrix such that there are always some electrically conducting ones to carry the current through. This is consistent with the SEM observation that an MWCNT network forms at the nanotube loading of 2.5 wt %. The conductivity increases continuously with increasing CNT content above this percolation threshold. The maximum conductivity was 5.16 S/cm for the nanocomposites with 15 wt % MWCNTs.

The stability of the conductivity under stretching is critical for applications in stretchable electronic circuits. Figure 9 shows the conductivity as a function of mechanical deformation for the prepared nanocomposites with 5 and 15 wt % MWCNTs. For the sample with 5 wt % MWCNTs, the conductivity decreases continuously with increasing applied strain. In contrast, a clear plateau was observed for the sample with 15 wt % MWCNTs below the elongation of 50%, and the conductivity remains almost constant within this deformation range. Further increasing the strain leads to a decrease in conductivity. The stretching-induced decreasing of the electrical conductivity for nanocomposites containing CNTs has been reported in some previous studies, and it has been attributed to the breaking of the CNT network by mechanical deformation.[37,38] The CNTs are forced to align along the stretching direction by the external stress, and the electrical pathways are destroyed. The nanocomposite with 15 wt % MWCNTs has a very high entanglement density; thus, a small strain (<50%) cannot damage the MWCNTs network, and the electrical pathways are maintained. However, large deformation with a strain more than 50% results in the partial disrupture of the MWCNT network.

3.6. Cyclic Tensile Test. The deformation of the MWCNT network in the SEBS matrix upon mechanical stretching was also characterized by cyclic tensile tests. Successive tensile tests were performed on the nanocomposites with 5 and 15 wt % MWCNTs. Note that the sample is treated as a new sample with new dimensions in each tensile test, even if strain from the previous test remains. The measured moduli obtained from successive tensile tests are listed in Table 2. For the nanocomposite with 5 wt % MWCNTs, stress-softening behavior was observed over the whole deformation range, and the modulus of the nanocomposite decreased as the previously applied strains increased. However, for the nanocomposite with 15 wt % MWCNTs, only a slight decrease in the modulus of the sample was observed when a strain of less than 50% was previously applied, although stress-softening behavior was observed upon further increasing the previous strain (as shown in Table 2). This mechanical behavior upon stretching is highly consistent with the results of the conductivity measurements shown in Figure 9. The MWCNT entanglement density in the two samples appears to account for the observed mechanical and electrical performance. Small MWCNT loading (such as 5 wt %) produces limited nanotube entanglement, and the resulting MWCNT network was broken even at a low strain. For the sample with a high MWCNT content, the rigid MWCNT network is basically unchanged at a low strain, but further stretching induces the alignment of the nanotubes and leads to the breaking of the MWCNT network in the nanocomposite.

4. Conclusions

Pristine MWCNTs can be uniformly dispersed in an SEBS matrix using a high-shear extruder with a screw rotation speed of 1000 rpm. The dispersed MWCNTs form a network upon more than 2.5 wt % loading, and the entanglement increases with increasing nanotube loading. There is strong interfacial adhesion between the nanotube surface with the matrix. Therefore, stretchable (with a stretchability of more than 600%), elastic (with a strain recovery of more than 60% for a preset strain of 200%), and electrically conductive elastomer composites were fabricated upon the addition of more than 2.5 wt % MWCNTs. The nanocomposite with a very high MWCNT loading of 15 wt % exhibits excellent conductivity stability upon uniaxial deformation with a strain of less than 50%. Further stretching induces the disruption of the MWCNT network, which results in both a decrease in electrical conductivity and mechanical stress-softening. In addition, the well-dispersed MWCNTs have a marked effect on the phase separation behavior of the matrix block copolymer. They inhibit the local phase separation of SEBS, and the MWCNT network impedes the formation of large phase-separated grains; thus, a lower order−disorder transition temperature was observed for the nanocomposites than that for neat SEBS.

References and Notes

(1) Norman, R. H. *Conductive Rubber and Plastics*; Elsevier: London, 1970.
(2) Sichel, E. K. *Carbon Black-Polymer Composites*; Marcel Dekker: New York, 1982.
(3) Khang, D. Y.; Jiang, H. Q.; Huang, Y.; Rogers, J. A. *Science* **2006**, *311*, 208–212.
(4) Kim, D. H.; Ahn, J. H.; Choi, W. M.; Kim, H. S.; Kim, T. H.; Song, J.; Huang, Y. Y.; Liu, Z.; Lu, C.; Rogers, J. A. *Science* **2008**, *320*, 507–511.
(5) Haggenmuller, R.; Guthy, C.; Lukes, J. P.; Fischer, J. E.; Winey, K. I. *Macromolecules* **2007**, *40*, 2417–2421.
(6) Mitchell, C. A.; Krishnamoorti, R. *Macromolecules* **2007**, *40*, 1538–1545.
(7) Li, Y. J.; Shimizu, H. *Macromolecules* **2008**, *41*, 5339–5344.
(8) Pegel, S.; Pötschke, P.; Petzold, G.; Alig, I.; Dudkin, S. M.; Lellinger, D. *Polymer* **2008**, *49*, 974–984.
(9) Pötschke, P.; Dudkin, S. M.; Alig, I. *Polymer* **2003**, *44*, 5023–5030.
(10) Pötschke, P.; Abdel-Goad, M.; Alig, I.; Dudkin, S. M.; Lellinger, D. *Polymer* **2004**, *45*, 8863–8870.
(11) Zhang, Q. H.; Rastogi, S.; Chen, D. J.; Lippits, D.; Lemstra, P. J. *Carbon* **2006**, *44*, 778–785.
(12) Koerner, H.; Liu, W.; Alexander, M.; Mirau, P.; Dowty, H.; Vaia, R. A. *Polymer* **2005**, *46*, 4405–4420.
(13) Koerner, H.; Price, G.; Pierce, N. A.; Alexander, M.; Vaia, R. A. *Nat. Mater.* **2004**, *3*, 115–120.
(14) Sekitani, T.; Noguchi, Y.; Hata, K.; Fukushima, T.; Aida, T.; Someya, T. *Science* **2008**, *321*, 1468–1472.
(15) Khang, D. Y.; Xiao, J.; Kocabas, C.; MacLaren, S.; Banks, T.; Jiang, H.; Huang, Y. Y.; Rogers, J. A. *Nano Lett.* **2008**, *8*, 124–130.
(16) Xiao, J.; Jiang, H.; Khang, D. Y.; Wu, J.; Huang, Y.; Rogers, J. A. *J. Appl. Phys.* **2008**, *104*, 033543.
(17) Chen, G. X.; Li, Y. J.; Shimizu, H. *Carbon* **2007**, *45*, 2334–2340.
(18) Li, Y. J.; Shimizu, H. *Polymer* **2007**, *48*, 2203–2207.
(19) Shimizu, H.; Li, Y. J. *Macromolecules* **2005**, *38*, 7880–7883.
(20) Masuda, J.; Torkelson, J. M. *Macromolecules* **2008**, *41*, 5974–5977.
(21) Kim, J. K.; Lee, H. H.; Sakurai, S.; Aida, S.; Masamoto, J.; Nomura, S.; Kitagawa, Y.; Suda, Y. *Macromolecules* **1999**, *32*, 6707–6717.
(22) Jeong, U.; Lee, H. H.; Yang, H.; Kim, J. K.; Okamoto, S.; Aida, S.; Sakurai, S. *Macromolecules* **2003**, *36*, 1685–1693.
(23) Hamley, I. W. *The Physics of Block Copolymers*; Oxford University Press: New York, 1998.
(24) Hjji, P.; David, L.; Gerard, J. F.; Pascault, J. P.; Vigier, G. *J. Polym. Sci., Polym. Phys.* **1999**, *37*, 3127–3187.
(25) Ganguly, A.; Bhowmick, A. K.; Li, Y. J. *Macromolecules* **2008**, *41*, 6246–6253.
(26) Brus, J.; Spirkova, M.; Hlavata, D.; Strachota, A. *Macromolecules* **2004**, *37*, 1346–1357.
(27) Drazkowski, D. B.; Lee, A.; Haddad, T. S.; Cookson, D. J. *Macromolecules* **2006**, *39*, 2854–2863.
(28) Drazkowski, D. B.; Lee, A.; Haddad, T. S. *Macromolecules* **2007**, *40*, 2798–2805.
(29) Cheng, C. F.; Cheng, H. H.; Cheng, P. W.; Lee, Y. J. *Macromolecules* **2006**, *39*, 7583–7590.
(30) Liu, Y. L.; Hsu, C. Y.; Wei, W. L.; Jeng, R. J. *Polymer* **2003**, *44*, 5159–5167.
(31) Agag, T.; Koga, T.; Takeichi, T. *Polymer* **2001**, *42*, 3399–3408.
(32) Kojima, Y.; Usuki, A.; Kawasumi, M.; Okada, A.; Fukushima, Y.; Kurauchi, Y.; Kamigaito, O. *J. Mater. Res.* **1993**, *8*, 1185–1189.
(33) Kumar, S.; Jog, J. P.; Natarajan, U. *J. Appl. Polym. Sci.* **2003**, *89*, 1186–1194.
(34) Wu, J.; Hwang, K. C.; Huang, Y. *J. Mech. Phys. Solids* **2008**, *56*, 279–292.
(35) Xiao, K. Q.; Zhang, L. C.; Zarudi, I. *Compos. Sci. Technol.* **2007**, *67*, 177–182.
(36) Yasmin, A.; Luo, J. J.; Abot, J. L.; Daniel, I. M. *Compos. Sci. Technol.* **2006**, *66*, 2415–2422.
(37) Du, F. M.; Fischer, J. E.; Winey, K. I. *Phys. Rev. B* **2005**, *72*, 121404–121407.
(38) Lanticse, L. J.; Tanabe, Y.; Matsui, K.; Kaburagi, Y.; Suda, K.; Hoteida, M.; Endo, M.; Yasuda, E. *Carbon* **2006**, *44*, 3078–3086.

MA802662C